



**HAL**  
open science

## Thermo-mechanical behavior of energy diaphragm wall: physical and numerical modelling

Shengshi Dong, Xiaozhao Li, Anh Minh A.M. Tang, Jean-Michel Pereira, van  
Tri Nguyen, Ping Che, Zhiyong Xiong

► **To cite this version:**

Shengshi Dong, Xiaozhao Li, Anh Minh A.M. Tang, Jean-Michel Pereira, van Tri Nguyen, et al..  
Thermo-mechanical behavior of energy diaphragm wall: physical and numerical modelling. Applied  
Thermal Engineering, 2019, 10.1016/j.applthermaleng.2018.09.054 . hal-02877008v2

**HAL Id: hal-02877008**

**<https://enpc.hal.science/hal-02877008v2>**

Submitted on 23 Jun 2020

**HAL** is a multi-disciplinary open access archive for the deposit and dissemination of scientific research documents, whether they are published or not. The documents may come from teaching and research institutions in France or abroad, or from public or private research centers.

L'archive ouverte pluridisciplinaire **HAL**, est destinée au dépôt et à la diffusion de documents scientifiques de niveau recherche, publiés ou non, émanant des établissements d'enseignement et de recherche français ou étrangers, des laboratoires publics ou privés.

1 **Thermo-mechanical behavior of energy diaphragm wall: physical**  
2 **and numerical modelling**

3 Shengshi DONG<sup>a</sup>, Xiaozhao LI<sup>a</sup>, Anh Minh TANG<sup>b</sup>, Jean Michel PEREIRA<sup>b</sup>, Van Tri

4 NGUYEN<sup>b</sup>, Ping CHE<sup>c</sup>, Zhiyong XIONG<sup>a</sup>

5 *<sup>a</sup> School of Earth Sciences and Engineering, Nanjing University, Zhugongshan Building, Xianlin*  
6 *Avenue, Nanjing, Jiangsu Province 210023, PR China*

7 *<sup>b</sup> Laboratoire Navier, UMR 8205, École des Ponts ParisTech, IFSTTAR, CNRS, UPE, France*

8 *<sup>c</sup> East China Mineral Exploration and Development Bureau, Nanjing, Jiangsu Province 210007,*  
9 *PR China*

10

11 Corresponding author:

12 Xiaozhao LI

13

14 Nanjing University

15 No.163 Xianlin Avenue, Nanjing

16 210023 Jiangsu Province

17 PR China

18 Email : [lixz@nju.edu.cn](mailto:lixz@nju.edu.cn)

19 Phone : +86 13951604941

20 **Abstract:** The paper presents a study of the thermo-mechanical behavior of energy diaphragm  
21 wall. A physical model, which consists of a small-scale concrete diaphragm wall equipped with  
22 a heating exchange pipe, was used. A heating test was performed where hot water (at 50 °C) was  
23 circulated through a heat exchange pipe for 75 h. The results show that the temperatures in the  
24 wall and in the soil increased quickly during the first 20 h and reached stabilization at the end of  
25 the experiment. Heating induced increase of axial strain in the wall and earth pressure at the  
26 soil/wall interface. In addition to the experiment, a numerical model, using finite element  
27 analysis, was used to predict the behavior of the wall during this experiment. The good  
28 agreement between the numerical and the experimental results allows the main phenomena that  
29 took place to be explained; heating induces thermal expansion of the wall that results in the  
30 modification in stress in the wall and at the soil/wall interface. In addition, since the pipe was  
31 located closer to one side of the wall, the thermal expansion of the wall was not homogenous,  
32 and the wall bent during heating.

33 **Keywords:** Thermo-mechanical behavior; Energy diaphragm wall; Physical model; Numerical  
34 simulation

35

## 36 **1. Introduction**

37 A thermo-active (or energy) geostructure is a new-style Ground Source Heat Pump (GHSP)  
38 system that consists of conventional geostructures (*e.g.* pile foundation, tunnel lining, diaphragm  
39 wall) with individual or several pipe circuits (high-density polyethylene pipes, HDPE) of  
40 primary circuit embedded within to enable heat exchange with the surrounding ground [1]. In  
41 winter, heat is extracted from the ground for the purpose of heating and in summer, heat is  
42 injected into the ground to provide cooling. Energy geostructures are considered an interesting  
43 and promising technology to tackle the increasing energy demands for heating and cooling of  
44 buildings and other infrastructures, by making use of it as a local and sustainable source.  
45 However, there are still concerns about the thermal exchange, between the structure and the  
46 ground, which may induce variation in the stress/strain behavior of the geostructure and, as a  
47 consequence, be a threat to its safety and performance. Thus, several research works have been  
48 focused on the thermo-mechanical behavior of energy geostructures in order to better understand  
49 its stress/strain behavior under combined thermal and mechanical loading [2-8].

50

51 However, most of the existing studies are related to the thermo-mechanical behavior of energy  
52 piles. The methods used include in situ experiments [9-12], laboratory tests [13-23] and  
53 numerical simulations [24-29]. It has been reported that there are significant changes in stress  
54 distribution and shaft resistance due to constraints on the thermal expansion/contraction [30].  
55 Although these phenomena are not expected to lead to detrimental consequences, they should be  
56 taken into consideration at the design stage.

57

58 Few studies of the thermo-mechanical performance of energy diaphragm walls have been  
59 published however [31, 32]. It has been suggested that thermally-induced strains and stresses  
60 also develop in energy walls [32]. However, their effects are less predictable than in energy piles  
61 because of their greater complexity in terms of geometry. Sterpi *et al.* [32] performed 3D  
62 thermo-mechanical Finite Element Analyses (FEA) and concluded that the thermally induced  
63 effects on the structure were not negligible and could be observed partly as additional  
64 displacements, partly as variations of the internal actions. Bourne-Webb *et al.* [31] also  
65 performed numerical simulations and found that changes to the wall mechanical response were  
66 dominated by seasonal temperature changes.

67

68 The most important function of the diaphragm wall is for ground support and seepage control. If  
69 there is crack in the wall, the deformation caused by thermal expansion/contraction and lateral  
70 soil pressure may aggravate the damage. Some diaphragm walls are also applied for bearing  
71 purpose, as a result, the thermally-induced strains and stresses are thus important to be  
72 investigated. Numerical analysis have demonstrated an increase of radial contact pressures on  
73 the soil-pile interface due to temperature-induced expansion of the pile [33, 34]. For energy pile,  
74 this increase of radial contact pressures could only increase the soil-pile frictional resistance. But  
75 for diaphragm wall, due to the existence of excavation at one side of the wall, the pressure  
76 change may cause additional deformation after Sterpi *et al.* [32]. However, the bending moment  
77 caused by heating was small and overwhelmed by the effect of environmental thermal boundary

78 conditions through numerical analysis by Bourne-Webb *et al.* [31].

79

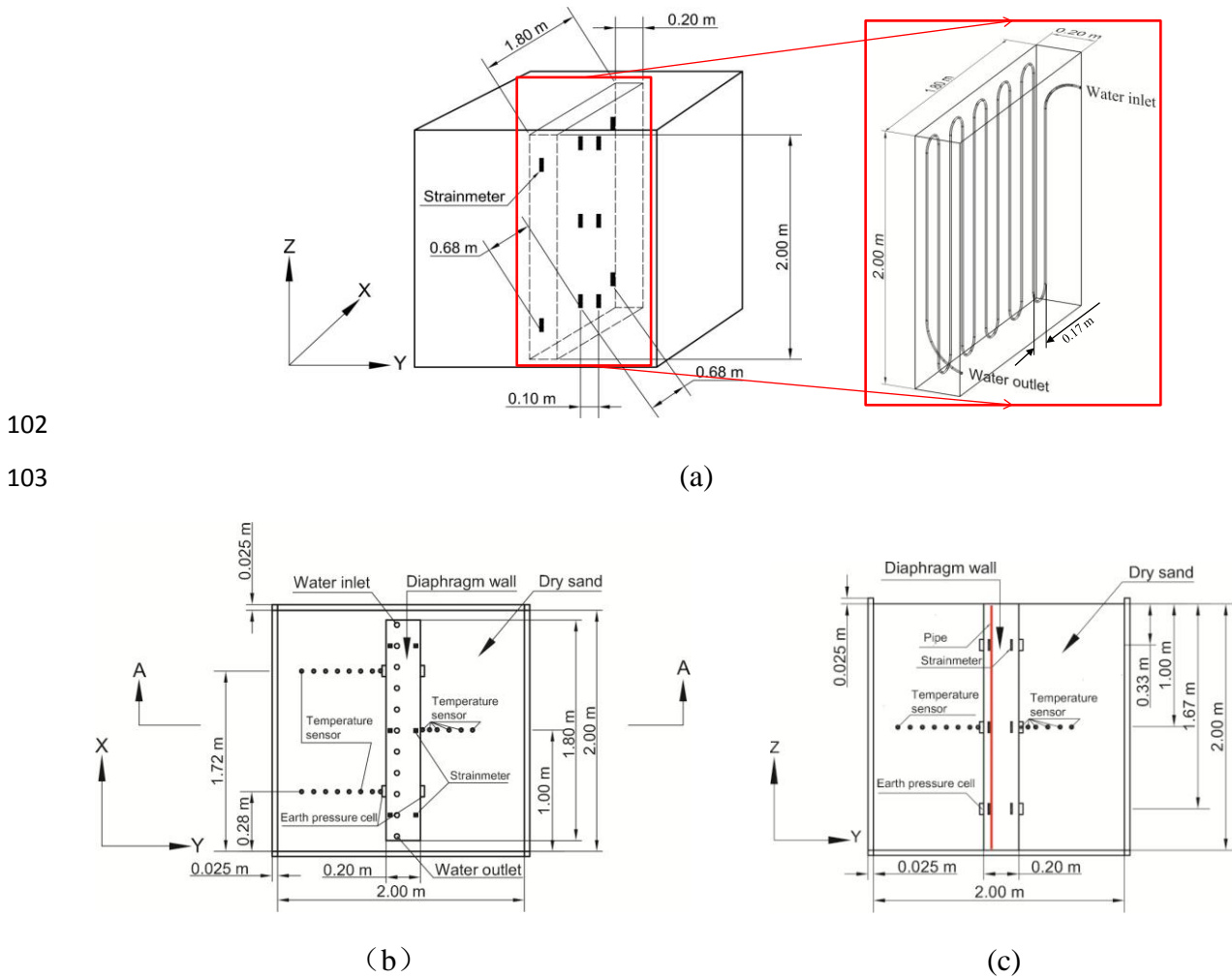
80 This paper presents a study to evaluate the thermo-mechanical response of an energy diaphragm  
81 wall by using physical and numerical modeling. A small-scale energy diaphragm wall was  
82 installed in dry sand. Its behavior under thermal loading was monitored using strain, stress and  
83 temperature sensors embedded inside/on the wall and also in the surrounding soil. At the same  
84 time, its behavior was predicted by using Finite Element Analyses (FEA). The combination of  
85 the two methods allows better understanding the thermo-mechanical behavior of an energy  
86 diaphragm wall when its temperature is varied.

87

## 88 **2. Physical model**

89 The schematic view of the physical model is shown in Figure 1. A small-scale concrete  
90 diaphragm wall (2.00 m high, 1.80 m wide, and 0.20 m thick) was installed inside a steel box  
91 and the bottom of the wall was in contact with the bottom of the box. The internal height and  
92 width of the box are similar to those of the wall. The thickness of the box walls and floor is 25  
93 mm with other 30 mm grillage structure outside, which is large enough to consider that the box  
94 is rigid. The box was exposed to the indoor air with a controlled temperature of  $10 \pm 2^\circ\text{C}$  and  
95 the heat convection between the surfaces and air is natural convection. Prior to the experiment,  
96 the box was filled with dry sand in layers of 0.2-m thickness which were compacted to a density  
97 of about  $1.62 \text{ Mg/m}^3$  (corresponding to a relative density of 80% and void ratio of 0.63). The  
98 control of density by layer ensures its uniformity throughout the test specimen. This physical

99 model can be considered representative of the wall below the internal excavation level. As a  
 100 result, the effect of the thermal boundary conditions on the thermo-mechanical behavior,  
 101 identified in other studies [30, 31], will not be captured.



104 Fig. 1. Schematic view of the experimental setup; (a) 3D view of the physical model with the  
 105 details of the pipe and strainmeters; (b) Horizontal section at Z = 1.00 m; (c) Section A-A,  
 106 Vertical section at X = 1.00 m.

107  
108 The soil temperature was measured at various locations located on a plane at 1-m depth (see

109 Figure 1c). At this depth, the temperature sensors were distributed in three lines, two on the  
 110 left-hand side and one on the right-hand side (see Figure 1b). This allows the soil temperature to  
 111 be measured at different distances from the diaphragm wall surfaces at the same depth. The  
 112 diaphragm wall was equipped with high-density polyethylene pipes (10 mm in external diameter  
 113 and 8 mm in internal diameter) to distribute the heating fluid, and various sensors to measure  
 114 earth pressure, temperature and strain. The details are shown in Figures 1. The pipes were  
 115 distributed on a plan located at 0.05 m from the left-hand side surface of the wall and the  
 116 distance between the pipes was 0.17 m (see Figure 1b, c). The details of the pipe arrangement  
 117 are shown in Figure 1a. To measure the earth pressure at the soil/wall interface, 12 sensors were  
 118 used. These sensors were distributed at three depths (0.33 m, 1.00 m, and 1.67 m) (see Figure  
 119 1c). At each depth, two sensors were located on each side of the wall (see Figure 1b). Several  
 120 strainmeters were tied to the rebars, as shown in Figure 1a, to measure the strain at various  
 121 locations inside the wall. Note that the strainmeters and the earth pressure transducers have  
 122 integrated with thermistors to measure the temperature. The characteristics of the sensors used  
 123 are shown in Table 1 and the calibration and correction for the temperature were done by the  
 124 producers and considered in the data processing. The wall was fabricated outside of the box.  
 125 After 30 days of curing, it was then installed inside the box and the earth pressure and soil  
 126 temperature sensors were installed during the compaction of dry sand to fill the box.

127

128 Table 1. Detailed information of sensors

Sensor	Market model No.	Specification	Capacity	Sensibility	Error
--------	------------------	---------------	----------	-------------	-------

Earth pressure cell	JTM-V2000	Vibrating wire	300 kPa	$\leq 0.24$ kPa	$\leq 1$ kPa
Strainmeter (embedment)	BGK-4200	Vibrating wire	3000 $\mu\epsilon$	1 $\mu\epsilon$	$\leq 3$ $\mu\epsilon$
Temperature sensor	Pt100	Thermal resistance	0-300 °C	$\leq 0.04\%$	0.3 °C

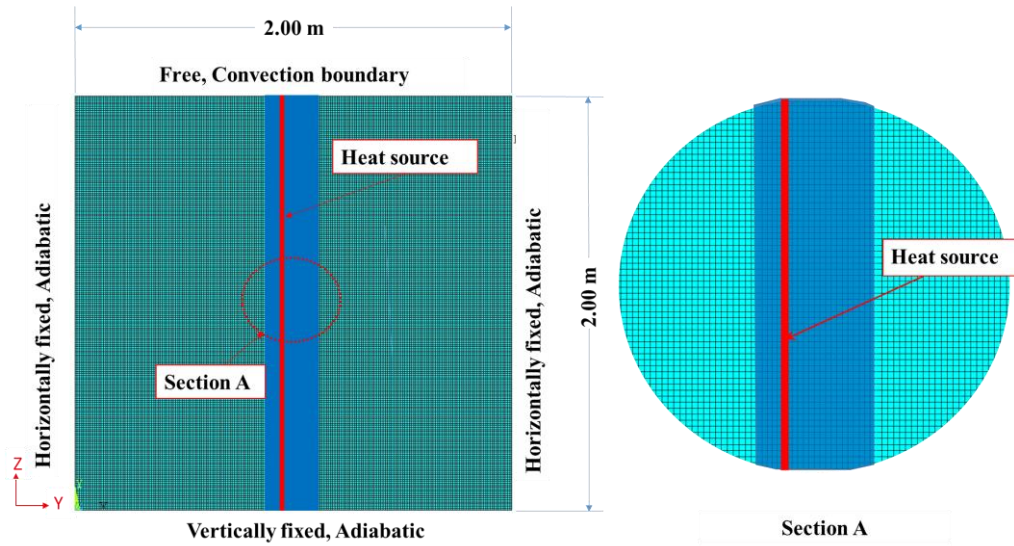
129

130 After the installation of the experiment, heating was applied to the wall by circulating water  
 131 through the pipes at a temperature of 50 °C and with a flow rate of 0.03 m<sup>3</sup>/h for a period of 75  
 132 h. Beside the temperature evolution which was measured at various locations inside the wall and  
 133 in the soil, earth pressures at the soil/wall interface and strains inside the wall were also  
 134 recorded.

### 135 **3. Numerical model**

136 In order to predict the mechanical behavior of the wall during this experiment, Finite Element  
 137 Analysis (FEA) (using ANSYS) was under taken. The 2D mesh, plotted in Figure 2, represents  
 138 the section shown in Figure 1c. Plane strain conditions were applied corresponding to the  
 139 boundary conditions of the experiment. The horizontal displacements at the left-hand side and  
 140 the right-hand side were restrained. The vertical displacement at the bottom of the mesh was  
 141 also restrained while the stress applied to the top of the mesh was null. The downward vertical  
 142 displacement of the base of the wall was restrained but the horizontal displacement was not.  
 143 According to the experimental results, the thermal boundary conditions on the left-hand side and  
 144 right-hand side have only small influence on the temperature distribution. For this reason, the  
 145 thermal boundary conditions on these two sides were supposed to be adiabatic. Heat flux was

146 equally supposed to be negligible at the bottom boundary. On the top of the model, thermal  
147 convection boundary was set with an air temperature of 10 °C and a convective heat transfer  
148 coefficient of 2.5 W/(m<sup>2</sup>.K)([31]), as it was open to the air.



149  
150 Fig.2 Finite element mesh and boundaries conditions used for the numerical simulations.

151  
152 The governing laws used in this study are summarized as follows: (i) only conduction was  
153 considered for heat transfer; (ii) the mechanical behavior of the wall was linear elastic while that  
154 of the soil was elasto-plastic with the Drucker-Prager yield criterion; (iii) the thermo-mechanical  
155 behavior of the wall and soil was linear elastic. The material parameters used for the simulation  
156 are shown in the Table 2. Among the parameters, the density, thermal conductivity and specific  
157 heat of cement mortar and sand used in the FEA were measured by specialized equipment and  
158 also calibrated by one dimensional finite difference method with MATLAB. The Young's  
159 modulus and Poisson's ratio of cement mortar were measured by elastic modulus test machine.

160 Other parameters of cement mortar and sand were taken from the literatures ([35-37]). It should  
 161 be stated that the coefficient of linear expansion was chosen at  $0.6 \times 10^{-5} \text{ } ^\circ\text{C}^{-1}$  from literature  
 162 [35], which gives a typical linear thermal expansion coefficient for dense quartzose sands from  
 163  $0.6 \times 10^{-5} \text{ } ^\circ\text{C}^{-1}$  to  $2.0 \times 10^{-5} \text{ } ^\circ\text{C}^{-1}$ . The lowest value was chosen to examine the effects of soil  
 164 thermal expansion on the thermal-mechanical behavior of the wall. For the friction angle, there  
 165 are literatures which give  $30\text{-}36^\circ$  from loose sand to dense sand [36, 38], we chose  $30^\circ$  as it's  
 166 density may not easy to compacted to the design stage of the lower depth. According to  
 167 literature review [36], the dilation angle of dense sand and loose sand are from  $0\text{-}12^\circ$  and  $0\text{-}10^\circ$ ,  
 168 respectively. It was chosen at  $4^\circ$  as an intermediate value in the present study.

169

170 Table 2. Materials parameters used for simulation

Parameter	Cement mortar	Dry sand
Thermal conductivity (W/(m.K))	1.20	0.32
Density ( $\text{Mg/m}^3$ )	1.55	1.62
Specific heat (J/(kg.K))	736	700
Young's modulus (MPa)	12,000	50
Poisson's ratio (-)	0.20	0.23
Coefficient of linear expansion ( $\mu\text{E}/^\circ\text{C}$ )	10	6
Cohesion (kPa)	—	0.1
Friction angle ( $^\circ$ )	—	30

171

172 In order to simulate the heating phase performed in the experiment, the temperature of the pipes  
173 (the vertical line located inside the wall, see Figure 2) was imposed. The initial temperature of  
174 the whole system was first fixed at 10 °C (following the experimental observation). To start the  
175 heating phase, the temperature of the pipe was increased from 10 °C to 48.5 °C following  
176 function (1):

$$177 \quad T = \frac{2.07 \bullet t + 1.1615}{0.0414 \bullet t + 0.12323} \quad (1)$$

178 where  $t$  is elapsed time and  $T$  is temperature. This choice allows fitting the experimental data of  
179 the temperature measured by the sensor that is closest to the pipes (0.03 m from the pipe axis, on  
180 the left-hand side).

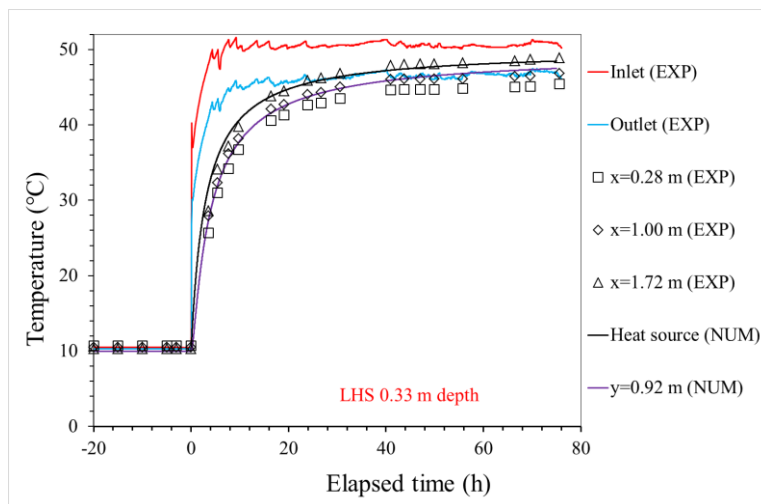
#### 181 **4. Result**

182 In this section, the results obtained from physical test and numerical analysis are compared in  
183 the same figures.

184 Figure 3 shows the temperature measured within the wall on the left-hand side in the plane of  
185 the wall panel at three different depths (0.33 m, 1.00 m and 1.67 m) and on the right-hand side at  
186 mid-plane ( $x = 1.00$  m Fig.1) versus elapsed time (the origin corresponds to the start of the  
187 heating phase). The symbols represent the experimental data (EXP) and the continuous lines  
188 represent the numerical results (NUM). Note that in the experiments, more than one sensor  
189 exists for one distance (see Figure 1b). As an example, at  $y=0.92$  m on the left-hand side (Figure

190 3) within the wall, there are three sensors on each depth (0.33 m and 1.67 m). The results  
191 obtained by these three sensors (showing an increase of temperature from 10 °C to 45 °C) have a  
192 difference of about 3-4 °C at the end of the heating phase. This difference can be explained by  
193 the gradual cooling of the fluid while circulating into the pipe which represents an ordinary  
194 characteristic condition of energy diaphragm wall.

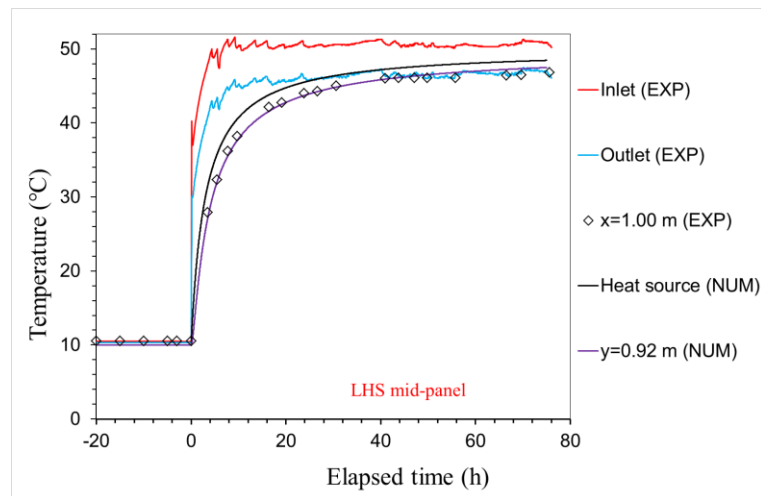
195



196

197

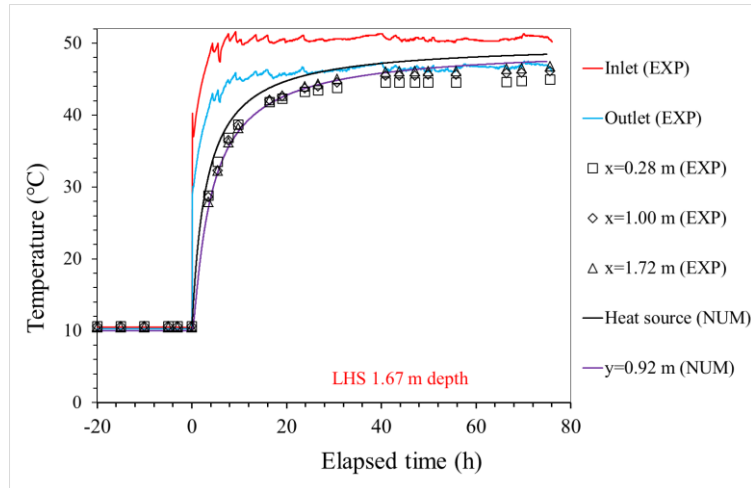
(a)



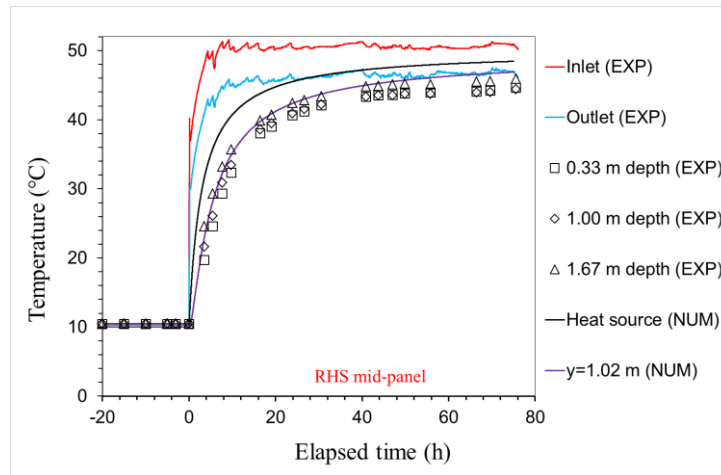
198

199

(b)



(c)



(d)

200  
201

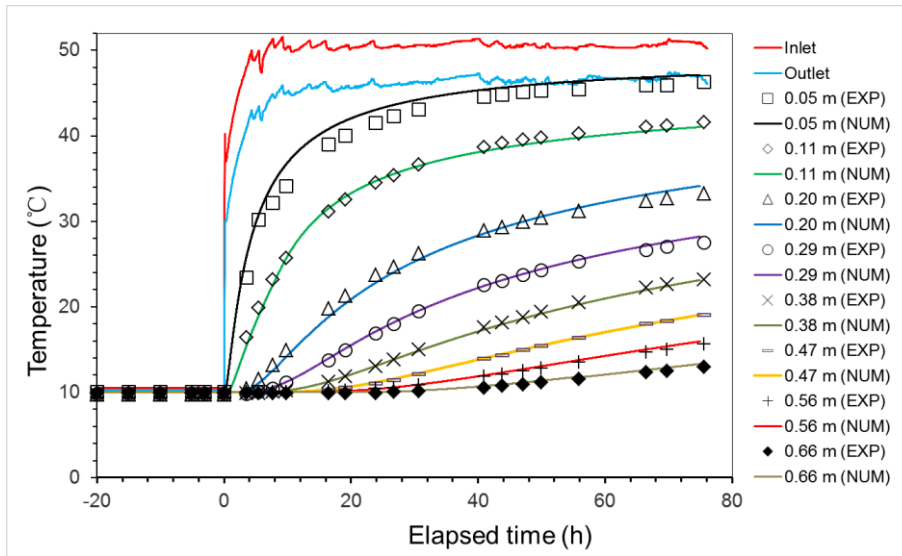
202  
203

204 Fig.3. Temperature versus elapsed time within the wall on the left-hand side along the x  
205 coordinate at depth of (a) 0.33 m and (b) 1.00 m and (c) 1.67 m and on the right-hand side at  
206 x=1.00 m for various depths (d)

207

208 Figure 4 shows the temperature for each single line of sensors embedded in the sand. The  
209 agreement between the experimental data and the numerical results confirms that the numerical  
210 2D finite element model is suitable to predict the heat transfer in sand in this experiment.

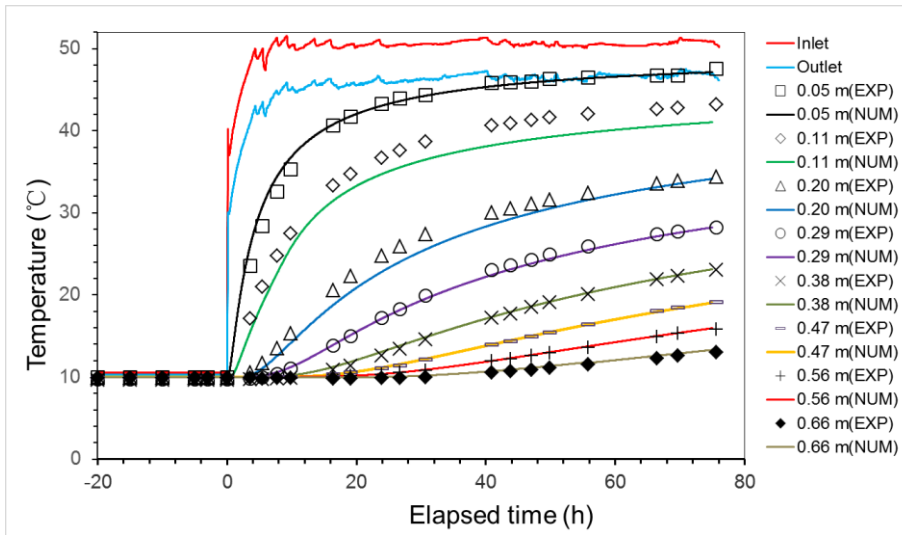
211



212

213

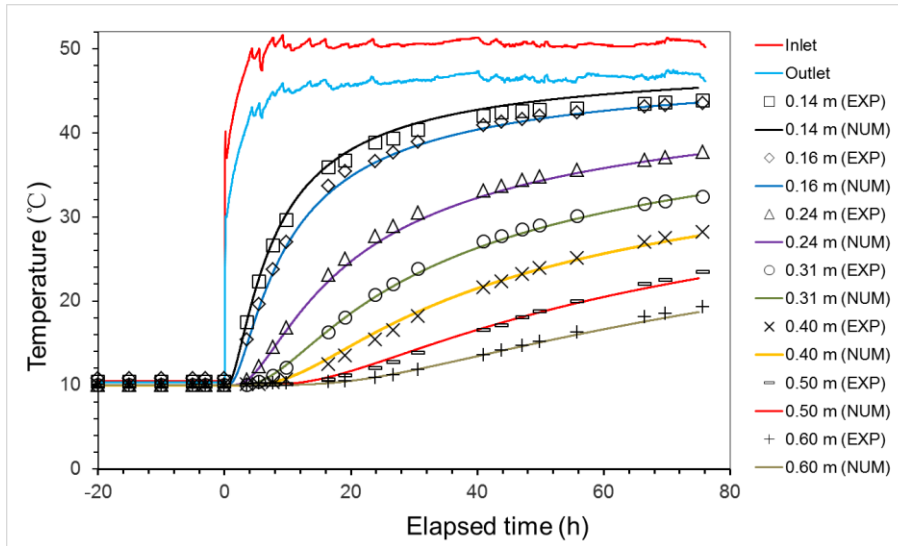
(a)



214

215

(b)



(c)

216

217

218 Fig.4. Temperature versus elapsed time in the sand mass at various distances from the pipes axis:

219 (a) on the left-hand side at  $x = 0.44$  m; (b) on the left hand side at  $x = 1.56$  m; (c) and on the

220 right-hand side at  $x = 1.00$  m.

221

222 Figure 5 shows the temperature profile measured at various moments. It can be seen that at a

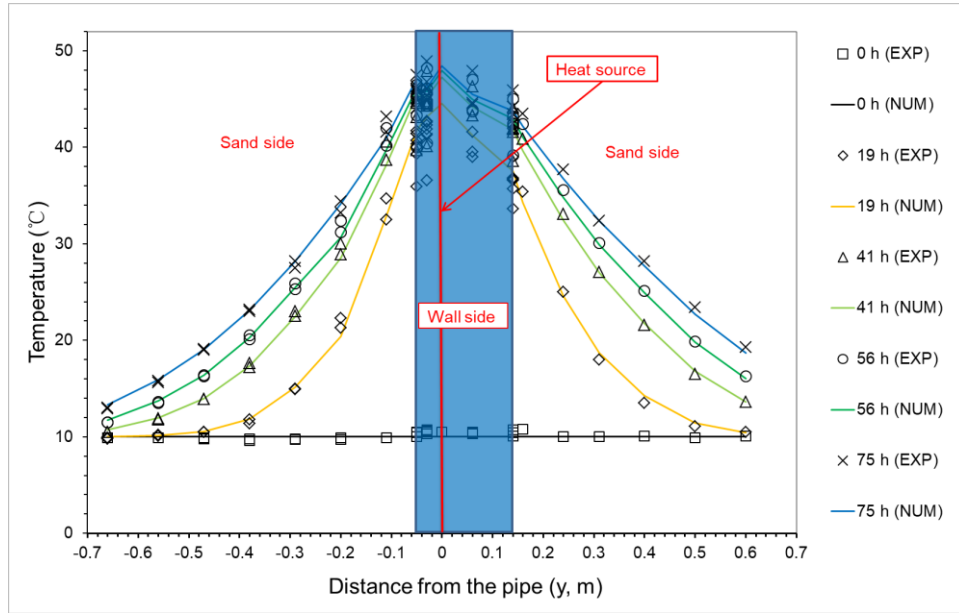
223 given time, the temperature at a location closer to the pipe is higher. This plot allows two zones

224 to be distinguished: inside the wall, the temperature gradient is smaller than in the soil. That can

225 be explained by the thermal conductivities of these materials and the boundary conditions: the

226 wall, made of cement, is more conductive than the sand and therefore, the temperature gradient

227 is then smaller.



228

229 Fig.5 Temperature versus distance from the pipe at various elapsed times in the middle of the  
 230 panel ( $z=1.00$  m)

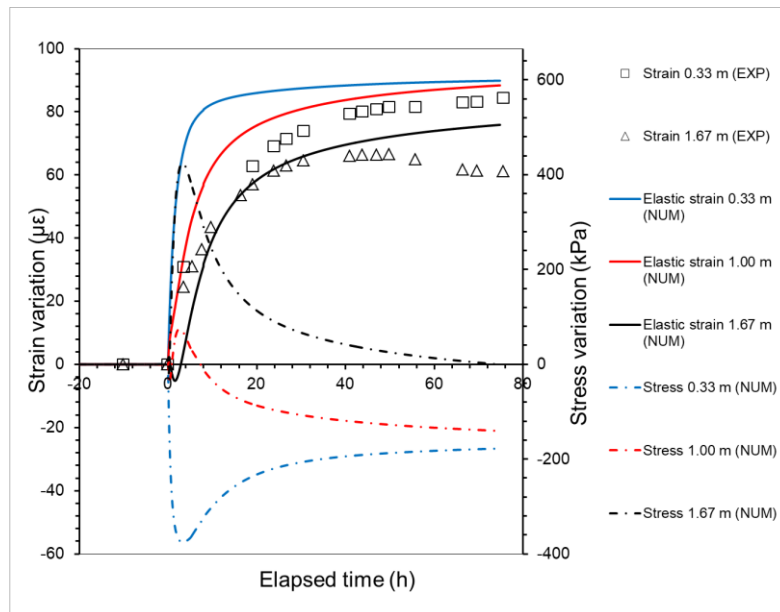
231

232 The numerical results shown in Figures 3, 4 and 5 are in good agreement with the experimental  
 233 results. That confirms, in this experiment, heat transfer is mainly governed by heat conduction  
 234 (as considered in the numerical simulation). This agreement confirms also that the thermal  
 235 boundary conditions used in the simulation are acceptable. In addition, as a 2D mesh was used  
 236 in the simulation, the numerical results should be compared with the mean values obtained in the  
 237 experiments with various sensors located at the same distance. The non-uniform of the  
 238 temperature distribution along the X direction (observed from the experiments) can be ignored  
 239 in the numerical model.

240

241 Figure 6 shows the vertical strain (Z direction, see Figure 1a) measured at various x coordinates  
 242 by the strainmeters. Note that all the strainmeters on the left-hand side (Figure 6a, 6b and 6c) are  
 243 located 0.03 m from the pipe. The results show similar trends for all sensors; a rapid increase of  
 244 strain during the first 20 h (corresponding to the increase of fluid temperature during the  
 245 experiment) followed by a more stable phase. The final strain is in the range of 50-70  $\mu\epsilon$  (except  
 246 one sensor at 0.33-m depth). The three sensors located at 0.33-m depth show larger strain  
 247 variation than those at 1.67-m depth; there is only one sensor located at 1.00-m depth. On the  
 248 right-hand side (Figure 6d), only one sensor was used for each depth. Note that these sensors are  
 249 located 0.06 m to the right-hand side of the pipes. The results obtained by these sensors are quite  
 250 similar showing a quick increase during the first 20 h and stabilization at 55 - 65  $\mu\epsilon$ . These  
 251 discrepancies in strains can be directly linked to the heterogeneity of temperature distribution of  
 252 the wall shown in Figure 6.

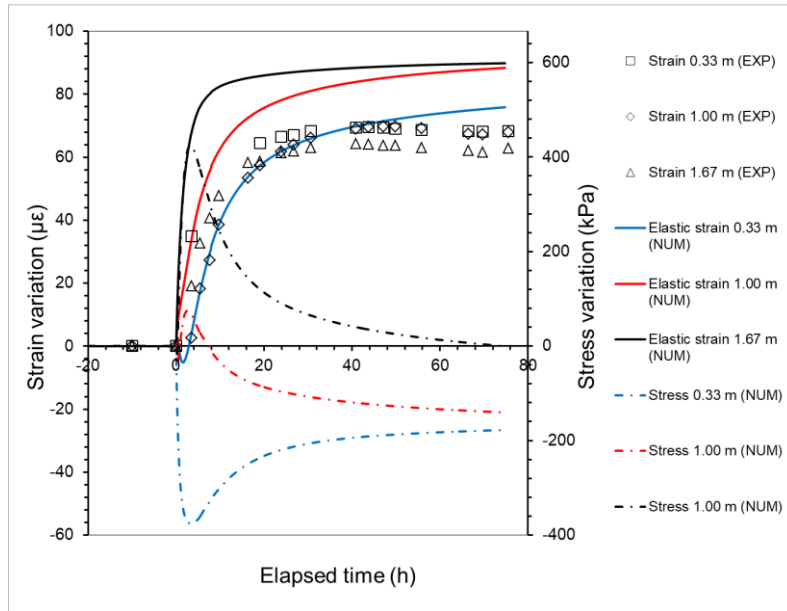
253



254

255

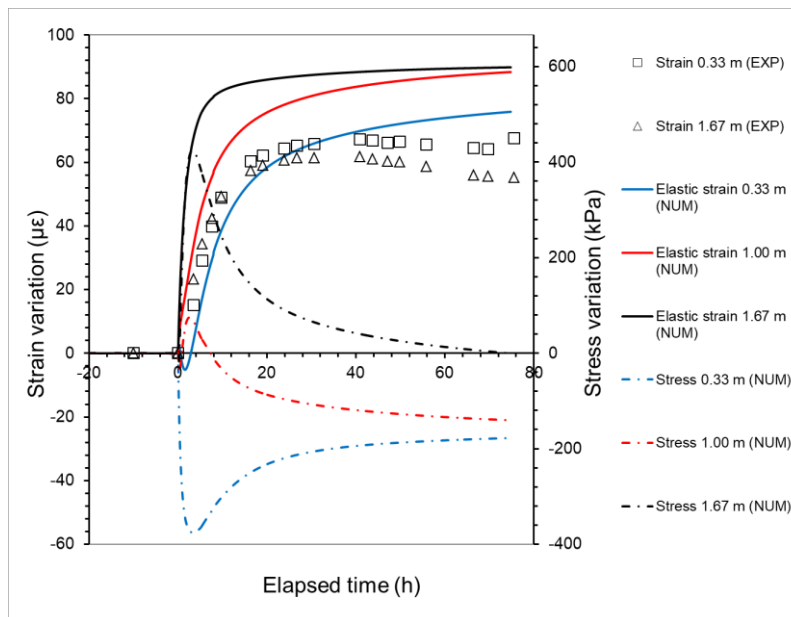
(a)



256

257

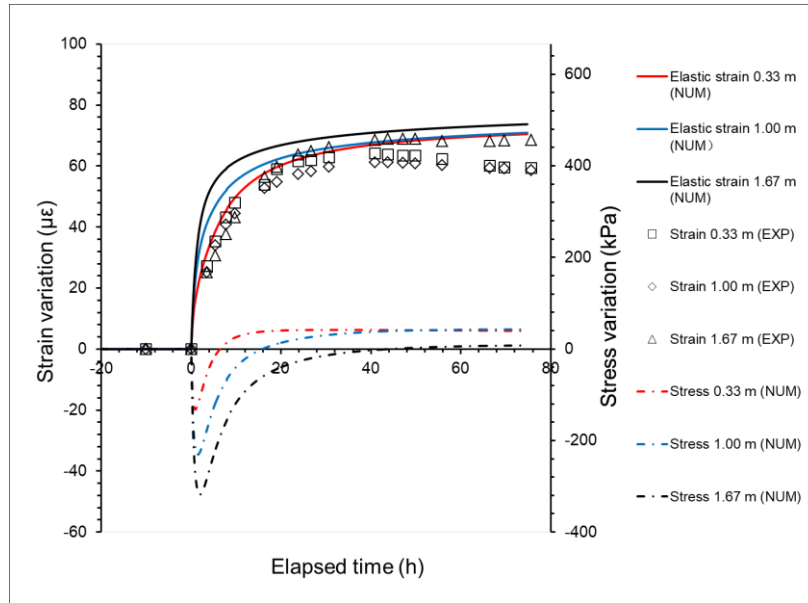
(b)



258

259

(c)



(d)

260

261

262 Fig.6. Vertical strain and stress versus elapsed time on the left-hand side at (a)  $x=0.28$  m ; (b)  $x$   
 263  $= 1.00$  m ; (c)  $x=1.72$  m ; (d) and on the right hand at  $x=1.00$  m.

264

265

266 The vertical strains predicted by the numerical analysis are also shown in the Figure 6 (positive  
 267 strain corresponds to expansion). On the left-hand side, the numerical analysis show that heating  
 268 induced a quick expansion at 0.33-m depth followed by stabilization at  $80 \mu\epsilon$ . This result is  
 269 similar to that obtained by the experiment. However, for the other depth (1.67 m), the numerical  
 270 analysis shows a contraction during the first hours. This contraction was then followed by  
 271 expansion and the final values are also similar to the experimental ones. The trend of the vertical  
 272 strains on the right-hand side shows a good agreement between the numerical and the  
 273 experimental results.

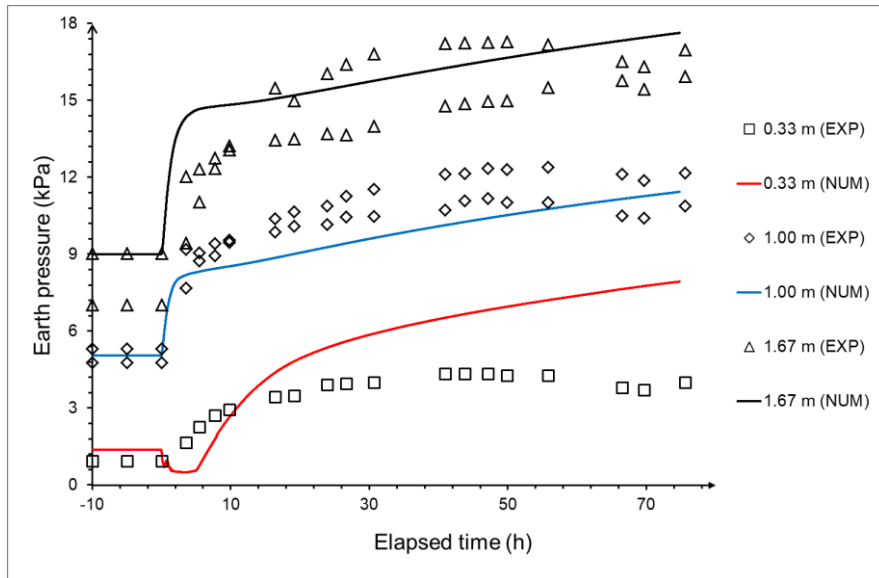
274

275 The following mechanisms can be mentioned to explain these results (see also the vertical stress  
276 variation plotted in the Figure 6). The high value of vertical stress is related to the temperature  
277 gradient in the wall thickness (see Figure 1). When the temperature of the wall increases, the  
278 vertical strain increases by the thermal expansion. As the boundary condition at base of the  
279 domain was vertically fixed, the deformation of the wall could only expand upward. On the  
280 left-hand side, the heating rate is higher (so during the first 20 h), thermal expansion on the  
281 left-hand side is higher than the right-hand side. This thermal expansion in the left-hand side  
282 was then "restrained" by the right-hand side of the wall. At the same time, the vertical expansion  
283 of the wall mobilizes the shaft friction along its interface in contact with the soil mass. That  
284 mobilized shaft friction tends to prevent the wall vertical expansion, increasing then the vertical  
285 stress inside the wall. On the other hand, the sensors located at larger depths (1.67 m) are  
286 subjected to higher increase of vertical stress. That explains the compression of the wall during  
287 the first hours on the left-hand side at large depths and tensile stress on the right-hand side.

288

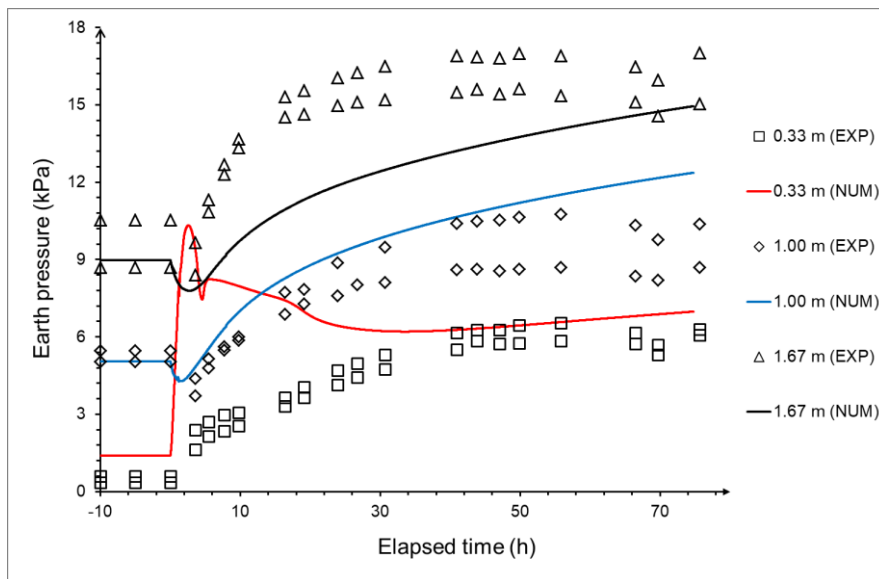
289 Figure 7 shows the normal stress on soil-wall interface versus elapsed time at various locations.  
290 The initial value of the lateral earth pressure is approximately 1 kPa at 0.33 m depth, 5 kPa at  
291 1.00 m depth and 9 kPa at 1.67 m depth. On the left-hand side (Figure 7a), at 0.33-m depth,  
292 there is only one transducer. The measurement shows a quick increase of the earth pressure  
293 following the heating phase, and the value at stabilization is approximately 4 kPa. At 1.00-m  
294 depth, there are two sensors both showing a quick increase of the earth pressure and the final  
295 values are approximately 11 kPa. The discrepancies between the two sensors are around 1 kPa.

296 The sensors at 1.67-m depth show similar trend with the final values close to 16 kPa. As a  
 297 conclusion, for the left-hand side, the variation of earth pressure is more significant at greater  
 298 depth during heating.



299  
 300

(a)



301  
 302

(b)

303 Fig.7 Stress versus elapsed time at various depths on the left-hand side (a) and on the  
 304 right-hand side (b).

305

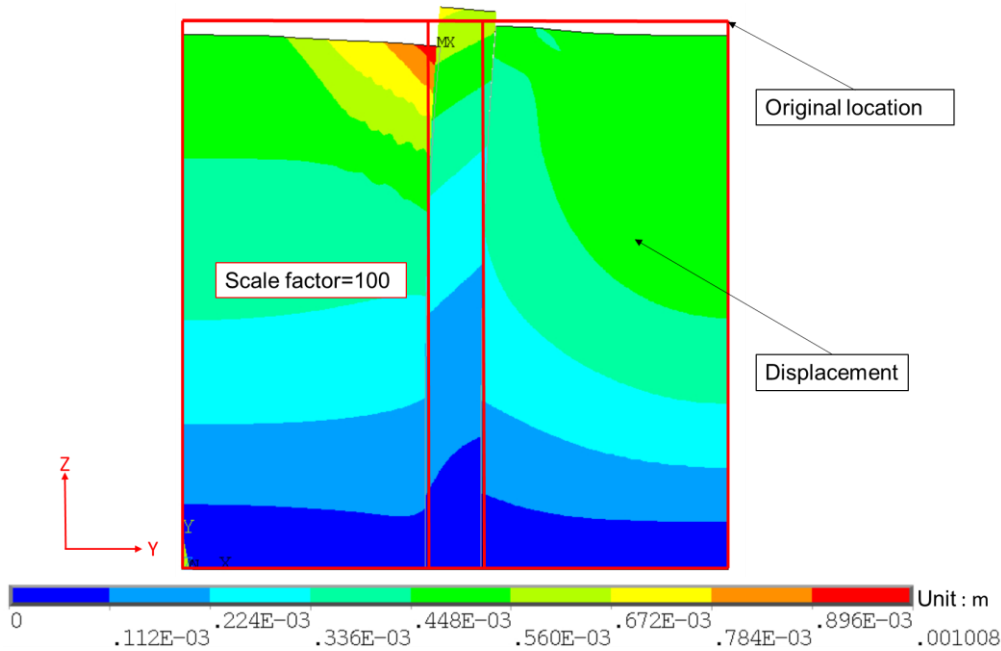
306 The general trend observed on the right-hand side is different at the start of heating (Figure 7b).  
307 At 0.33-m depth, the two earth pressure sensors show quick increase with the heating and the  
308 final average value equals 6 kPa, with a discrepancy of less than 0.5 kPa. At 1.00-m depth, both  
309 sensors show first a decrease of the earth pressure during the first hours of heating. These values  
310 increase and reach around 9 kPa at the end (with a discrepancy of 1 kPa). For the sensors at  
311 1.67-m depth, the earth pressure increases with the heating and reaches 15 -17 kPa at the end. It  
312 could be seen there are still increase of pressure on both side at end of the test, this may due to a  
313 minor problem with the measurement.

314

315 The numerical results corresponding to the sensors at 1.00-m and 1.67-m depths show good  
316 agreement with the experimental ones for both sides. Even the decrease of the earth pressure at  
317 1.00-m depth on the right-hand side was well predicted. However, the numerical results  
318 corresponding to lower depth (0.33 m) are significantly different from the experiment values.  
319 On the left-hand side, the numerical simulation shows a decrease of earth pressure during the  
320 first hour, which was not observed in the experiment. On the right-hand side, the earth pressure  
321 spikes during the first hour, which was not observed in the experiment. These problems would  
322 be explained by the mechanical behavior of the sand in higher deflections [36, 39] under low  
323 stress level that could not be well predicted by FEA. This could also explain why was there  
324 reasonable accord before heating.

325

326 In order to better understand the results on the change of earth pressure (shown in Figure 7), the  
327 deformed mesh (5 h after the starting of the heating) is shown in Figure 8. Heating induces  
328 thermal expansion of the wall. That tends to increase the earth pressure at the soil/wall interface.  
329 However, as the pipes were located closer to the left-hand side, the temperature distribution is  
330 non-uniform. With the temperature on the left-hand side increasing more quickly than that on  
331 the right-hand side. This induces a bending of the wall that can be seen clearly in the Figure 9.  
332 This bending contributes also to the modification of the earth pressure. Besides the increase of  
333 earth pressure related to the wall expansion, the wall bending decreases the earth pressure  
334 (mostly on the top) on the left-hand side and increases that on the right-hand side. That explains  
335 why the increase of earth pressure at 0.33-m depth on the right-hand side is higher than those at  
336 higher depth and the order is opposite on the left-hand side. In addition, the bending of the wall  
337 also explains the decrease of earth pressure observed at 1.00-m depth on the right-hand side  
338 during the first few hours.



339  
 340 Fig.8 Deformed mesh at 5 hours (the color represents the sum of Y and Z displacement  
 341 vectors).

342

343 **5. Discussion**

344 In the present work, a 1-g physical model was used to study the thermo-mechanical behavior of  
 345 an energy wall panel. Strainmeters were used to capture the axial strain inside the wall and earth  
 346 pressure transducers were used to capture the normal stress at the soil/wall interface. This  
 347 approach has been used in various studies to investigate the mechanical behavior of  
 348 geostuctures [40-42]. The results obtained in the present work show that this method could be  
 349 also used to investigate the thermo-mechanical behavior of energy geostuctures.

350

351 As far as the numerical model was concerned, the present study used a plane strain 2D FE model  
 352 that approximates the conditions of the experiment. Even if this model could not capture the 3D

353 heterogeneity of the temperature distribution, related to the difference between the inlet and  
354 outlet temperatures, a generally good agreement between the numerical and the experimental  
355 results can be observed. This confirms also that the boundary conditions and the constitutive  
356 laws used in this model are suitable for this case. Note that, for studying the thermal behavior of  
357 energy geostructures, usually only heat conduction is considered for heat transfer in the soil and  
358 in the reinforce concrete [29, 30, 43] unless ground water flow is present [7, 44, 45]. Heat  
359 convection in heat exchange pipe was discussed in the literature [32] and the heat transfer  
360 mechanism between the fluid and the pipe is more complex to be simulated [46, 47]. The  
361 hypothesis of elastic deformation is usually used for gravel soils in numerical simulation  
362 because it is in agreement with experimental observations [27, 29, 48, 49]. In some cases where  
363 clayey soils were considered, more complex constitutive laws maybe required [50-53]. As  
364 mentioned above, to simplify the model, the heat exchange pipe is often represented by a line  
365 with controlled temperature [26]; The thermo-mechanical behavior of the soil was assumed to  
366 be elastic and the effect of temperature on the soil mechanical properties was ignored.

367

368 Both numerical and experimental results obtained in the present work evidence that heating the  
369 diaphragm wall induces thermal expansion and this increases the lateral earth pressure applied  
370 on the wall surface. The lateral earth pressure could be three times larger than the initial stress  
371 value under low stress level. This variation seems to have a significant contribution to the  
372 vertical stress within the wall. Previous studies on energy pile indicate that radial contact

373 pressures typically increase less than 5 kPa along 20 m depth of the pile under an increase of 25°C  
374 of the pile temperature [33, 34]. In real scale structures, the height to width ratio could be much  
375 higher than the ratio in this physical study (equal to 10). As a result, the increase of lateral earth  
376 pressures might be negligible with respect to the variations of vertical stresses. However, for an  
377 energy pile, the increase of this pressure is almost homogenous because the layout of the pipes is  
378 usually symmetric. For diaphragm walls, the behavior is more complex and strongly depends on  
379 the distribution of the heat exchange pipes inside the wall. The eccentric position of the heat  
380 exchanger loop caused a temperature gradient across the wall thickness, which leads to wall  
381 bending. This phenomenon exists also in the wall that is not fully embedded [31], since the  
382 temperature condition on the soil side is different from the temperature condition on the  
383 excavation side. This represents an additional contribution to thermally-induced vertical strains  
384 that are not uniform on the two sides of the wall.

385

## 386 **6. Conclusions**

387 The thermo-mechanical behavior of energy wall panel during heating was investigated using  
388 both physical and numerical models. The following conclusions can be drawn:

389

- 390 - Heating induces thermal expansion of the wall. The vertical thermal expansion mobilizes  
391 the shaft friction between the soil and the wall and then modifies the axial stress state inside  
392 the wall. Horizontal expansion increases the earth pressure at the soil/wall interface, and

393 thus increases the mobilized shaft friction along the wall and the vertical stress inside the  
394 wall.

395 - As the pipe layout was not symmetric, thermal expansion bends the wall resulting in  
396 different stress/strain response between the two sides.

397 - A short-term heating of the wall shows a significant temperature gradient across the wall  
398 thickness. As a result, significant stress/strain variation is generated within the wall during  
399 the first few hours.

400 - The numerical model using an elastic law for the thermo-mechanical behavior of soil is  
401 appropriate to predict the behavior of the wall under thermal loading. There is however  
402 some discrepancy between experiment and numerical results that requires a deeper  
403 investigation, i.e. soil behavior at low stress level, 3D effect in the numerical model, etc.

404 - In spite of the temperature difference between the outlet and inlet fluid temperature, that  
405 induced a non-uniform temperature distribution inside the wall, a 2D numerical model  
406 seems appropriate to predict the main features of the panel's thermo-mechanical behavior  
407 observed by physical model.

408

#### 409 **Acknowledgement**

410 This research was supported by the National Natural Science Foundation of China (grant  
411 number 41272314); and Science and Technology Project of Suzhou (grant number  
412 SYG201451); and the European Commission via the Marie Curie IRSES project GREAT  
413 'Geotechnical and geological Responses to climate change: Exchanging Approaches and

414 Technologies on a world-wide scale' (grant number FP7-PEOPLE-2013-IRSES-612665).

415 Thanks are also due to Yinkang Zhou from Nanjing University for valuable discussion.

416

## 417 **Reference**

418 [1] Brandl H (2006) Energy foundations and other thermo-active ground structures.

419 GEOTECHNIQUE 56(2): 81-122. doi: 10.1680/geot.2006.56.2.81

420 [2] Laloui L, Nuth M (2008) Investigations on the mechanical behaviour of a Heat Exchanger

421 Pile. In: Deep Foundations On Bored And Auger Piles, Proceedings (No.

422 LMS-CONF-2009-003, pp 343-347). Crc Press-Taylor & Francis Group, 6000 Broken

423 Sound Parkway Nw, Ste 300, Boca Raton, Fl 33487-2742 Usa.

424 [3] Chuang YU, Pan LY, Liu SY, Cai YQ (2009) Working mechanism and application of heat

425 exchanger piles. Yantu Lixue/rock & Soil Mechanics 30(4):932-937. (In Chinese)

426 [4] Péron H, Knellwolf C, Laloui L (2011) A method for the geotechnical design of heat

427 exchanger piles In: Proceedings of the Geo-Frontiers 2011 Conference, Jie H, Daniel E,

428 Alzamora, PE ASTM, Geotechnical Special Publications (GSP) 211:470-479.

429 [5] Boënnec O (2009) Piling on the Energy. Geodrilling International 150:25-8.

430 [6] Dupray F, Li C, Laloui L (2014) Heat-exchanger piles for the de-icing of bridges. Acta

431 Geotech 9:413-423. doi: 10.1007/s11440-014-0307-2

432 [7] Suryatriyastuti ME, Mroueh H, Burlon S (2013) Impact of transient heat diffusion of a

433 thermoactive pile on the surrounding soil. In: Laloui L, Di Donna A (eds.) Energy

434 Geostructures: Innovation in Underground Engineering. ISTE Ltd. and John Wiley & Sons

- 435 Inc, 193-209.
- 436 [8] Kürten S, Mottaghy D, Ziegler M (2015) A new model for the description of the heat  
437 transfer for plane thermo-active geotechnical systems based on thermal resistances. *Acta*  
438 *Geotech* 10:219-229. doi: 10.1007/s11440-014-0311-6
- 439 [9] Laloui L, Nuth M, Vulliet L (2006) Experimental and numerical investigations of the  
440 behaviour of a heat exchanger pile. *Int J Numer Anal Met* 30(8):763-781. doi:  
441 10.1016/S1571-9960(05)80040-0
- 442 [10] Bourne-Webb PJ, Amatya B, Soga K, et al (2009) Energy pile test at Lambeth College,  
443 London: geotechnical and thermodynamic aspects of pile response to heat cycles.  
444 *Géotechnique* 59(3):237. doi: 10.1680/geot.2009.59.3.237
- 445 [11] McCartney JS, Murphy KD (2012) Strain Distributions in Full-Scale Energy Foundations  
446 (DFI Young Professor Paper Competition 2012). *DFI Journal-The Journal of the Deep*  
447 *Foundations Institute* 6(2):26-38. doi:10.1179/dfi.2012.008
- 448 [12] Murphy KD, McCartney JS, Henry KS (2015) Evaluation of thermo-mechanical and  
449 thermal behavior of full-scale energy foundations. *Acta Geotech* 10(2):179-195. doi:  
450 10.1007/s11440-013-0298-4
- 451 [13] Laloui L, Cekerevac C (2008) Non-isothermal plasticity model for cyclic behaviour of  
452 soils. *Int J Numer Anal Met* 32(5): 437-460. doi:10.1002/nag.629
- 453 [14] McCartney JS, Rosenberg JE, Sultanova A (2010) Engineering performance of  
454 thermo-active foundation systems. In: Goss CM, Kerrigan JB, Malamo J, McCarron MO,  
455 Wiltshire RL (eds) *GeoTrends: the Progress of Geological and Geotechnical Engineering*

- 456 in Colorado at the Cusp of a New Decade (GPP 6), 27–42.
- 457 [15] McCartney JS, Rosenberg JE (2011) Impact of heat exchange on the axial capacity of  
458 thermo-active foundations. In: Han J, Alzamora DE (eds) Proceedings of geo-frontiers  
459 2011 (GSP 211). ASCE, Reston, VA, 488–498
- 460 [16] Kalantidou A, Tang AM, Pereira J-M, Hassen G (2012) Preliminary study on the  
461 mechanical behaviour of heat exchanger pile in physical model. *Géotechnique*  
462 62(11):1047-1051. doi: 10.1680/geot.11.T.013
- 463 [17] Stewart MA, McCartney JS (2013) Centrifuge modeling of soil-structure interaction in  
464 energy foundations. *J Geotech Geoenviron* 140(4):04013044. doi:  
465 10.1061/(ASCE)GT.1943-5606.0001061
- 466 [18] Yavari N, Tang AM, Pereira J-M, Hassen G (2014) Experimental study on the mechanical  
467 behaviour of a heat exchanger pile using physical modelling. *Acta Geotech* 9(3):385-398.  
468 doi: 10.1007/s11440-014-0310-7
- 469 [19] Kramer CA, Ghasemi-Fare O, Basu P (2015) Laboratory thermal performance tests on a  
470 model heat exchanger pile in sand. *Geotech Geol Eng* 33(2):253-271. doi:  
471 10.1007/s10706-014-9786-z
- 472 [20] Goode III JC, McCartney JS (2015) Centrifuge modeling of end-restraint effects in  
473 energy foundations. *J Geotech Geoenviron* 141(8):04015034. doi:  
474 10.1061/(ASCE)GT.1943-5606.0001333
- 475 [21] Yavari N, Tang A.M, Pereira, J-M, Hassen G (2016) Mechanical behaviour of a  
476 small-scale energy pile in saturated clay. *Géotechnique* 66(11):878-887.

- 477 doi:10.1680/geot./15-T-026
- 478 [22] Yavari N, Tang AM, Pereira J-M, Hassen G (2016) Effect of temperature on the shear  
479 strength of soils and soil/structure interface. *Can Geotech J* 53(7):1186-1194. doi:  
480 10.1139/cgj-2015-0355
- 481 [23] Nguyen VT, Tang AM, Pereira J-M (2017) Long-term thermo-mechanical behavior of  
482 energy pile in dry sand. *Acta Geotech* 1-9. doi:10.1007/s11440-017-0539-z
- 483 [24] Laloui L, Nuth M (2005) Numerical modelling of the behaviour of a heat exchanger pile.  
484 *Revue européenne de génie civil* 9(5-6): 827-839.
- 485 [25] Rotta Loria AF, Gunawan A, Shi C, et al (2015) Numerical modelling of energy piles in  
486 saturated sand subjected to thermo-mechanical loads. *Geomech Eng En* 1:1-15.  
487 doi:10.1016/j.gete.2015.03.002
- 488 [26] Yavari N, Tang AM, Pereira JM, et al (2014) A simple method for numerical modelling of  
489 energy pile's mechanical behavior. *Géotechnique Lett* 4(April-June):119-124. doi:  
490 10.1680/geolett.13.00053
- 491 [27] Suryatriyastuti ME, Mroueh H, Burlon S (2012) Understanding the temperature-induced  
492 mechanical behaviour of energy pile foundations. *Renew Sust Energ Rev* 16(5):  
493 3344-3354. doi:10.1016/j.rser.2012.02.062
- 494 [28] Salciarini D, Ronchi F, Cattoni E, et al (2013) Thermomechanical effects induced by  
495 energy piles operation in a small piled raft. *Int J Geomech* 15(2):04014042.  
496 doi:10.1061/(ASCE)GM.1943-5622.0000375.
- 497 [29] Gashti EHN, Malaska M, Kujala K (2014) Evaluation of thermo-mechanical behaviour of

- 498 composite energy piles during heating/cooling operations. *Eng Struct* 75:363-373.  
499 doi:10.1016/j.engstruct.2014.06.018
- 500 [30] Amatya BL, Soga K, Bourne-Webb PJ, et al (2012) Thermo-mechanical behaviour of  
501 energy piles. *Géotechnique* 62(6): 503-519. doi:10.1680/geot.10.P.116
- 502 [31] Bourne-Webb PJ, Freitas TMB, da Costa Gonçalves RA (2016) Thermal and mechanical  
503 aspects of the response of embedded retaining walls used as shallow geothermal heat  
504 exchangers. *Energ Buildings* 125:130-141. doi: 10.1016/j.enbuild.2016.04.075
- 505 [32] Sterpi D, Coletto A, Mauri L (2017) Investigation on the behaviour of a thermo-active  
506 diaphragm wall by thermo-mechanical analyses. *Geomech Eng En* 9:1-20. doi:  
507 10.1016/j.gete.2016.10.001
- 508 [33] Olgun CG, Ozudogru TY, Arson CF (2014) Thermo-mechanical radial expansion of heat  
509 exchanger piles and possible effects on contact pressures at pile–soil interface.  
510 *Géotechnique Lett* 4(3):170-178. doi:10.1680/geolett.14.00018
- 511 [34] Ozudogru TY, Olgun CG, Arson CF (2015) Analysis of friction induced  
512 thermo-mechanical stresses on a heat exchanger pile in isothermal soil. *Geotech Geol Eng*  
513 33(2):357-371. doi:10.1007/s10706-014-9821-0
- 514 [35] Yin S, Towler BF, Dusseault MB, et al (2009) Numerical experiments on oil sands shear  
515 dilation and permeability enhancement in a multiphase thermoporoelastoplasticity  
516 framework. *J Petrol Sci Eng* 69(3):219-226. doi:10.1016/j.petrol.2009.08.017
- 517 [36] Karthigeyan S, Ramakrishna V, Rajagopal K (2006) Influence of vertical load on the  
518 lateral response of piles in sand. *Comput Geotech* 33(2):121-131.

- 519 doi:10.1016/j.compgeo.2005.12.002
- 520 [37] Allan ML (2000) Materials characterization of superplasticized cement–sand grout.  
521 Cement Concrete Res 30(6):937-942. doi:10.1016/S0008-8846(00)00275-1
- 522 [38] Hazzar L, Nhussien M, Karray M (2017) Influence of vertical loads on lateral response of  
523 pile foundations in sands and clays. Journal of Rock Mechanics and Geotechnical  
524 Engineering 9(2):291-304. doi: 10.1016/j.jrmge.2016.09.002
- 525 [39] Hussien MN, Tobita T, Iai S, et al (2014) On the influence of vertical loads on the lateral  
526 response of pile foundation. Comput Geotech 55(1):392-403. doi:  
527 10.1016/j.compgeo.2013.09.022
- 528 [40] Reddy SB, Krishna AM (2015) Recycled Tire Chips Mixed with Sand as Lightweight  
529 Backfill Material in Retaining Wall Applications: An Experimental Investigation. Int J of  
530 Geosynth and Ground Eng 1(4):31. doi:10.1007/s40891-015-0036-0
- 531 [41] Lee KH, Cho JY, Salgado R, Lee I (2001) Retaining wall model test with waste foundry  
532 sand mixture backfill, Geotech Test J 24:401–408. doi: 10.1520/GTJ11137J
- 533 [42] Schad H, Vermeer PA, Lächler A (2007) Fresh concrete pressure in diaphragm wall panels  
534 and resulting deformations. In: Grosse, Ch. U. (Ed.): Advances in Construction Materials,  
535 Berlin: Springer Verlag, 2007:505-512.
- 536 [43] Sun M, Xia C, Zhang G (2013) Heat transfer model and design method for geothermal  
537 heat exchange tubes in diaphragm walls. Energ Buildings 61(6):250-259. doi:  
538 10.1016/j.enbuild.2013.02.017
- 539 [44] Di Donna A, Barla M (2016) The role of ground conditions on energy tunnels' heat

540 exchange. *ICE Env. Geotech.*, 3, 214-224. doi:10.1680/jenge.15.00030

541 [45] Dupray F, Baehler M, Laloui L (2013) Effect of groundwater flow on the THM behavior  
542 of an energy pile. *Proc. Int. Symp. Coupled Phenomena in Environmental Geotechnics*,  
543 Turin (Italy), 483-489. doi:10.1201/b15004-63

544 [46] Dubroca B, Duffa G, Leroy B (2002, September) High Temperature Mass and Heat  
545 Transfer Fluid-Solid Coupling. In *AIAA/AAAF 11th International Space Planes and*  
546 *Hypersonic Systems and Technologies Conference*, 5124.

547 [47] Khoury RRE, Errera M, Khoury KE, et al (2017) Efficiency of coupling schemes for the  
548 treatment of steady state fluid-structure thermal interactions. *Int J Therm Sci*  
549 115:225–235. doi: 10.1016/j.ijthermalsci.2017.02.001

550 [48] Jeong S, Lim H, Lee J K, et al (2014) Thermally induced mechanical response of energy  
551 piles in axially loaded pile groups. *Appl Therm Eng* 71(1):608-615.  
552 doi:10.1016/j.applthermaleng.2014.07.007

553 [49] Laloui L (2001) Thermo-mechanical behaviour of soils. *Revue Française De Génie Civil*  
554 5(6):809–843.

555 [50] Cekerevac C, Laloui L (2004) Experimental study of thermal effects on the mechanical  
556 behaviour of a clay. *Int J Numer Anal Met* 28(3):209-228. doi: 10.1002/nag.332

557 [51] Laloui L, Cekerevac C, François B (2005) Constitutive modelling of the thermo-plastic  
558 behaviour of soils. *Revue Européenne De Génie Civil* 9(5-6):635-650.

559 [52] Tang AM, Cui YJ, Barnel N (2008) Thermo-mechanical behaviour of a compacted  
560 swelling clay. *Géotechnique* 58(1):45-54. doi: 10.1680/geot.2008.58.1.45

561 [53] Hong PY, Pereira J-M, Tang AM, Cui YJ (2013) On some advanced thermo-mechanical  
562 models for saturated clays. *Int J Numer Anal Met* 37:2952 – 2971. doi: 10.1002/nag.2170

563